Convolution Analysis of Milling Force Pulsation

J.-J. Junz Wang*

Research Assistant.

S. Y. Liang

Assistant Professor.

W. J. Book

Professor.

George W. Woodruff School of Mechanical
Engineering,
Georgia Institute of Technology,
Atlanta, GA 30332-0405

This paper presents the establishment of a closed form expression for the dynamic forces as explicit functions of cutting parameters and tool/workpiece geometry in milling processes. Based on the existing local cutting force model, the generation of total cutting forces is formulated as the angular domain convolution of three cutting process component functions, namely the elementary cutting function, the chip width density function, and the tooth sequence function. The elemental cutting force function is related to the chip formation process in an elemental cutting area and it is characterized by the chip thickness variation, and radial cutting configuration. The chip width density function defines the chip width per unit cutter rotation along a cutter flute within the range of axial depth of cut. The tooth sequence function represents the spacing between flutes as well as their cutting sequence as the cutter rotates. The analysis of cutting forces is extended into the Fourier domain by taking the frequency multiplication of the transforms of the three component functions. Fourier series coefficients of the cutting forces are shown to be explicit algebraic functions of various tool parameters and cutting conditions. Numerical simulation results are presented in the frequency domain to illustrate the effects of various process parameters. A series of end milling experiments are performed and their results discussed to validate the analytical model.

1 Introduction

The fundamental understanding of the cutting force systems plays an important part in the monitoring, planning, and control of machining processes as well as in its traditional role in machine tool structure and servomechanisms design. Research in the kinematics of the milling process dates back to the work of Martellotti (1941, 1945). The basic cutter-chip thickness relationship takes the form of:

$$t_c(\theta) = t_x \sin(\theta) \qquad (1)$$

which is shown in Fig. 1. In this expression, the tooth trajectory of a milling cutter was assumed to be circular instead of trochoidal, therefore the equation is not an exact solution for the chip thickness. However, it is a good approximation when the feed per tooth is much less than the cutter diameter, and it has been widely used for the analysis of the milling process.

An empirical tangential cutting force equation for unit chip width is often written in an exponential form (Koenigsbergr, Sabberwal, 1961, 1962):

$$f_t(\theta) = C t_c(\theta)^{p+1}$$
$$= k_t(\theta) t_x \sin \theta, \text{ with } k_t(\theta) = C(t_x \sin \theta)^p \qquad (2)$$

A simplified model has been proposed by Sabberwal and Koenigsberger (1961) and used by many researchers (Kline et al., 1983; Fu et al., 1984; Tlusty and MacNeil, 1975; Subramani et al., 1987; Fussel and Srinivasan, 1989; Atantnis and Spence,

1991) to relate the tangential cutting force to the chip thickness for a unit chip width by the following form:

$$f_t = C_t(\bar{t}_c)^p t_x \sin \theta = K_t t_x \sin \theta \text{ with } K_t = C_t(\bar{t}_c)^p \qquad (3)$$

where K_t, the tangential cutting pressure constant, is related to the average chip thickness $\bar{t}_c$ and is often referred to as the average cutting pressure constant. Constants C, C_t, p, and therefore K_t are functions of tool edge geometry, the helical and rake angles, and tool/workpiece material properties. C_t and p in Eq. (3) are usually evaluated using the average cutting forces from experiments with various average chip thickness values.

Based on the local cutting force model, total cutting force models for the milling process have been derived by incorporating the considerations of cutter geometry, axial and radial depth of cut. Among these works were the establishment of
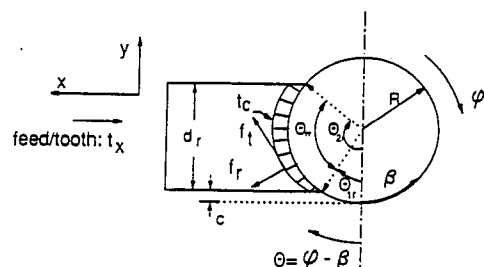
Fig. 1 Geometrical relationship between undeformed chip thickness (t_c), feed per tooth (t_x) and cutting forces ($f_t(\theta)$, $f_r(\theta)$)

closed form expressions for the total tangential cutting force on a single flute as a function of the cutter angular position (Koenigsberger and Sabberwal, 1961; Tlusty and MacNeil, 1975). Based on the single flute model, Koenigsberger and Sabberwal investigated the tangential cutting force pulsation during the multi-flute milling process and developed quantitative force relationships for slab and face millings within a certain range of cutting conditions. These relationships were evaluated and nomograms developed to show the magnitude of the average force and the ratio of maximum to average forces for different dimensions and positions of the cutter relative to the workpiece. Kato et al. (1981a, 1981b) experimentally investigated the relationships between cutting force variations and cutting conditions for plain milling operation with a single-toothed helical cutter and proposed a criterion for selecting the optimum cutting conditions to minimize the cutting force variation for a multi-toothed helical cutter.

In addition to Eq. (3), Tlusty and MacNeil (1975) related the radial cutting force to the tangential cutting force by a constant coefficient K_r:

$$f_r = K_r f_t \tag{4}$$

and examined the cutting force variation in end milling. It was experimentally observed that the cutting force responding to a sudden feedrate change can often be characterized by a time delay, which may give rise to instability in adaptive control. More recently, Yucesan et al. (1990) described elemental cutting force components in directions normal and parallel to the tool face. The three-dimensional total cutting forces were modeled in closed form using three process parameters: the normal pressure coefficient, friction coefficient, and the chip flow angle. Like K_t in Eq. (3), these parameters were assumed to be constants relating to the average chip thickness and average forces.

These cutting force models in the literature were based on the integration of local cutting forces with respect to the cutter angular position and different expressions were needed to evaluate forces at different angular conditions. Therefore the integration solutions were segmented into different formulations with different integration boundary points. Most of the integration expressions of the cutting force system applied to one cutter flute only. For a multi-flute cutter, care has to be taken to determine which flutes are engaged in the cutting and which appropriate integration form is to be used. Gygax conducted a detailed analysis (1979) and a series of experiments (1980) on the dynamics of single-tooth face milling under various cutting parameters. It was indicated that the extension from single-tooth to multi-tooth face milling could be achieved by convolution integration in the time domain. This is the first appearance of convolution modelling concept in the literature. However, no cutting force modelling technique was presented and more complicated milling situations were not treated.

With the abundance of computing resources in recent years, numerical integration has become a popular approach to modelling cutting forces. Kline, DeVor, and Lindberg (1982) developed mechanistic discrete models for end milling in which cutter is treated as an aggregation of discretized thin disk cutters along the cutter axis. At any angular position, chip load of each disk cutter can be computed as the product of chip thickness and disk thickness. Radial cutting constant K_r of Eq. (4) was treated like K_t of (3) as a function of average chip thickness $\bar{t}_c$ with

$$K_r = C_r (\bar{t}_c)_{p_r} \tag{5}$$

The effect of cutter runout is taken into consideration in forming revised chip thickness and average chip thickness expressions (Kline and DeVor, 1983). The associated cutting forces for the chip load of each disk can then be found from Eqs. (3) and (4). Summation of forces from all disks yields the total cutting forces. Sutherland and DeVor (1986) improved on the previous model by taking into account the effects of system deflection on the chip load. Following from Kline's model,

Nomenclature

α = cutter helical angle

$A_x[k], A_y[k]$ = Fourier coefficients at normalized frequency k of the total nominal x and y components cutting force, $\bar{f}_x, \bar{f}_y(\phi)$

β, r, h = angular, radius, and axial position variables for cutting point in the cutter cylindrical coordinate system

β_a = angular range of axial immersion of each flute within axial depth of cut

β_p = angular spacing between adjacent flutes, $2\pi/N$

c = workpiece recess

C_r = radial cutting coefficient

C_t = tangential cutting coefficient

$cwd(\beta)$ = chip width density function of a cutter flute

$cwd_c(\beta)$ = chip width density function of the cutter

D = cutter diameter

d_a, d_r = axial and radial depth of cut

ϕ = cutter angular displacement

$f_t, f_r(\theta)$ = tangential and radial local cutting forces per unit chip width

$\bar{f}_x, \bar{f}_y(\phi)$ = X and Y components of the total cutting force

$f_x, f_y(\theta)$ = X and Y components of the local cutting force per unit chip width with constant K_t and K_r

$f_{x1}, f_{y1}(\theta)$ = X and Y components of the local cutting force per unit chip width with variable k_t and k_r

η_a, η_c, η_r = β_a/β_p, c/D and d_r/D

K_t, K_r = average tangential cutting pressure constant and ratio of radial to tangential cutting force

k_t, k_r = variable tangential cutting pressure coefficient and ratio of radial to tangential cutting force

N = number of cutter flutes

p = tangential cutting force power law constant

$p_1(\theta), p_2(\theta)$ = X and Y components of the normalized tangential cutting force

p_r = radial cutting force power law constant

$p_t(\theta)$ = tangential elementary cutting function

$p_x(\theta), p_y(\theta)$ = elementary cutting functions in the X and Y directions

θ = cutting point angular position in the work

θ_{1r}, θ_{2r} = entry and exit angles determined from radial configuration

θ_{rr} = radial cutting range from radial configuration

R = cutter radius

$t_c(\theta)$ = uncut chip thickness

$\bar{t}_c$ = average chip thickness

$ts(\phi)$ = tooth sequence function

t_x = feed per tooth

ω = frequency normalized with respect to the spindle frequency

$w(\theta)$ = cutting window function for the radial cutting configuration

X, Y = the feed and normal directions in the work coordinate system

Note: Function variables in upper case letter are the Fourier transforms of the functions in lower case variable.

Fu, DeVor, and Kapoor (1984) developed a cutting force model for face milling which included the effects of spindle tilt and cutter runout. Alternatives to treat the elemental cutting forces differently were reported in the works of Zhou and Wang (1983), Ber et al. (1988), and Armarego and Deshpande (1989, 1991). Numerical integrations were commonly used in these formulations to compute the total milling forces.

Closed form frequency domain models provide alternative approaches to the study of effects of various cutting parameters on the different components of the total cutting forces. Based on the local cutting force model of Eqs. (3)–(5), this paper presents the work of establishing a closed form frequency domain expression for the cutting forces in milling as an explicit function of cutting parameters and tool/workpiece geometry through angular convolution modelling. The angular domain analysis is discussed in Section 2 and the frequency domain formulation in Section 3. Section 4 validates the analytical model based on experimental results and discusses the effect of using average cutting constants on the dynamic cutting force components.

2 Convolution Modelling of Multi-Tooth Milling Forces

In the following analysis the cutting force system at any instance of cutting is considered as the angular domain convolution of the cutting forces on any elemental point on the cutter, the width of chip produced during unit angular rotation of the cutter, and a periodic impulse train representing the sequence of tooth engagement. The derivation of these components, namely the elementary cutting function, the chip width density function, and the tooth sequence function, is discussed in detail in this section. Attention will be directed to the cases of ideal cutting with rigid cutter and workpiece in which cutting speed and feedrate are both constant while cutter runout and tilt do not exist, although deviations from ideal cases can be treated as well.

2.1 Elementary Cutting Functions. The analysis begins with considering an elemental cutting point on any flute of a multi-tooth cutter. As the cutter rotates, the point experiences a pattern of cutting forces as a function of the cutter angular position θ with respect to the workpiece. These force functions are described in Eqs. (3) and (4), which can be expressed in X and Y coordinates as follows:

$$\begin{pmatrix} f_x(\theta) \\ f_y(\theta) \end{pmatrix} = \begin{bmatrix} \cos\theta & \sin\theta \\ \sin\theta & -\cos\theta \end{bmatrix} \begin{pmatrix} f_t(\theta) \\ f_r(\theta) \end{pmatrix} \qquad (6)$$

where f_x and f_y represent the feed and normal forces, respectively. The elementary cutting functions in the X and Y directions, p_x and p_y, are defined as the normalized forces with respect to the maximum tangential cutting force $K_t t_x$. That is

$$p_x(\theta) = \frac{f_x(\theta)}{K_t t_x}$$

$$p_y(\theta) = \frac{f_y(\theta)}{K_t t_x} \qquad (7)$$

p_x and p_y thus are dimensionless functions of cutting point position in the work and can also be interpreted as the cutting forces acting on an elemental cutting area of unit chip width with unit feed per tooth per unit specific cutting pressure (K_t). From Eqs. (3)–(7), it can be shown that

$$\begin{pmatrix} p_x(\theta) \\ p_y(\theta) \end{pmatrix} = \begin{bmatrix} 1 & K_r \\ -K_r & 1 \end{bmatrix} \begin{pmatrix} p_1(\theta) \\ p_2(\theta) \end{pmatrix} \qquad (8)$$

where

$$p_1(\theta) = \frac{\sin 2\theta}{2}, \quad p_2(\theta) = \frac{1 - \cos 2\theta}{2} \qquad (9)$$

Notice that the cutting force expressions in (6) are applicable only over an angular range determined by the radial cutting configuration. This range of angular position is the difference between the cutter entry angle and the cutter exit angle as shown in Fig. 1. In the figure it can be seen that

$$\theta_{1r} = \cos^{-1}(1 - 2 * \eta_c)$$

$$\theta_{2r} = \cos^{-1}(1 - 2 * (\eta_r + \eta_c)) \qquad (10)$$

$$\theta_{rr} = \theta_{2r} - \theta_{1r}$$

where

$$\eta_r = \frac{d_r}{D} \text{ and } \eta_c = \frac{c}{D} \qquad (11)$$

A window function $w(\theta)$ can be defined as

$$w(\theta) = \begin{cases} 1, & \theta_{1r} \leq \theta \leq \theta_{2r} \\ 0, & \text{otherwise} \end{cases} \qquad (12)$$

With the definition of a window function, expression (9) can be rewritten in more precise terms as:

$$p_1(\theta) = \frac{\sin 2\theta}{2} w(\theta), \quad p_2(\theta) = \frac{1 - \cos 2\theta}{2} w(\theta) \qquad (13)$$

These elementary cutting functions, p_x and p_y, are the same for all cutting points anywhere on the cutter since they are defined with respect to a unit cutting area. The contributions of different cutting points on a flute to the total cutting forces differ only in the cutter angular displacement in which they engage in the cutting. Since cutting points on a flute engage in cutting in a predetermined sequence as dictated by the cutter geometry, these points produce orderly shifted functions of the same elemental cutting forces. The superposition of these shifted force functions sums to the total cutting forces for a single flute. Thus, we can treat the elemental cutting process as a linear shift-invariant system and think of the force functions generated at an elemental cutter point, namely p_x and p_y, as the cutting impulse response functions of the local cutting process in the X and Y directions. The system impulse response function has the cutter rotation displacement ϕ as its independent variable and represents the cutting force generated by a cutting point starting at $\phi = 0$. Assuming the cutting point is located at $\theta = 0$ when the cutter starts to rotate, the cutting point position in the work θ will be the same as the cutter rotation variable ϕ. Therefore, with a change of variable from θ to ϕ, Eq. (8) represents the system impulse response function of the local cutting process. The choice of cutting point position at $\phi = 0$ can be arbitrary as long as it is consistently used for other process functions. Choosing a different starting position will only cause a phase shift in the impulse response functions and the final total cutting forces.

One characteristic of a linear shift invariant system is that the system output can be obtained through convolution of its input function with the system impulse response, and more importantly, the frequency transform of the system output is the product of transforms of the input and system impulse response functions. These two properties of the linear shift invariant system form the basis of the model establishment and analysis of the milling force dynamics presented in this chapter.

2.2 Chip Width Density Function. The elementary cutting functions are defined with respect to a unit width of cut while the chip width density function, $cwd(\phi)$, discussed herein is concerned with the chip width produced by a flute during unit angular rotation of the cutter; therefore the chip width density function can be used to weigh each elemental force within the range of axial depth of cut. The *cwd* function for an arbitrary flute is defined with cutter rotation variable ϕ starting at 0 with the leading edge of that flute at $\beta = 0$
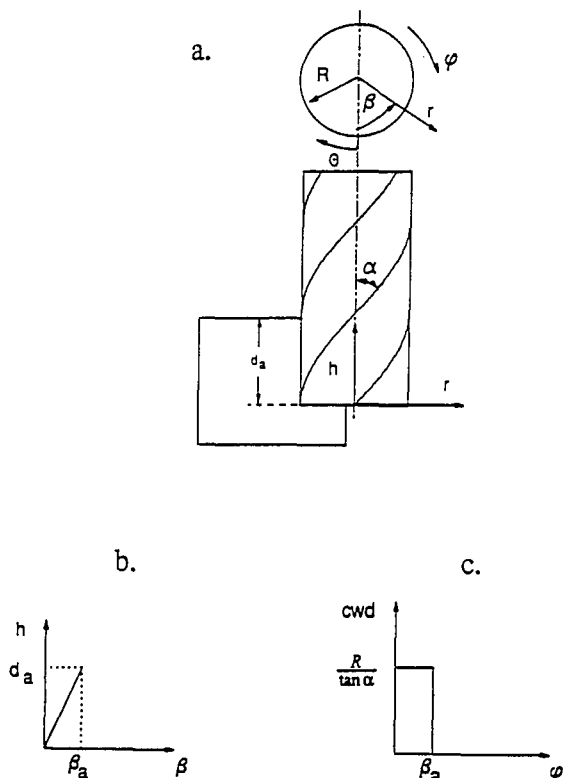
Fig. 2 Relationship between axial depth of cut and chip width density function

Fig. 3 The tooth sequence function

Fig. 4 Angular convolution model of total cutting force in X direction

positioned at $\theta = 0$, Fig. 2(a). It is therefore the chip width density observed at $\theta = 0$ as the cutter rotates. The chip width density function is determined from

$$cwd(\beta) = \frac{dh}{d\beta} \qquad (14)$$

where h is the axial position function for the chosen flute. Figure 2(b) shows the function $h(\beta)$ for a cutter flute with a constant helix angle α. Since the position variable β observed at $\theta = 0$ is essentially the same as cutter rotation variable ϕ, the chip width density function can be written as

$$cwd(\phi) = \begin{cases} \dfrac{R}{\tan \alpha} & 0 \le \phi \le \beta_a \\ 0, & \text{otherwise} \end{cases} \qquad (15)$$

where

$$\beta_a = \frac{d_a \tan \alpha}{R}$$

is the angular range of axial engagement. Equation (15) is a rectangular pulse function as shown in Fig. 2(c). The magnitude of this function is a constant dictated by the cutter geometry and the width of the rectangular pulse is determined by the axial depth of cut and the cutter geometry.

The chip width density function derived above is applicable to any flute on the cutter. As the milling cutter rotates, each flute will contribute to the total cutting force system through the same chip width density function except that the function is shifted by an angle equivalent to the spacing between flutes. Therefore, the chip width density function can again be treated as the impulse response of a linear shift-invariant process, which is termed the chip width generating process.

2.3 Tooth Sequence Function. For a cutter with evenly spaced flutes, the tooth sequence function can be determined from
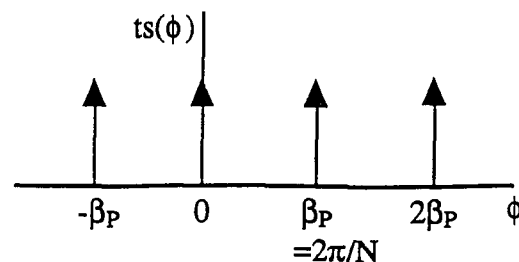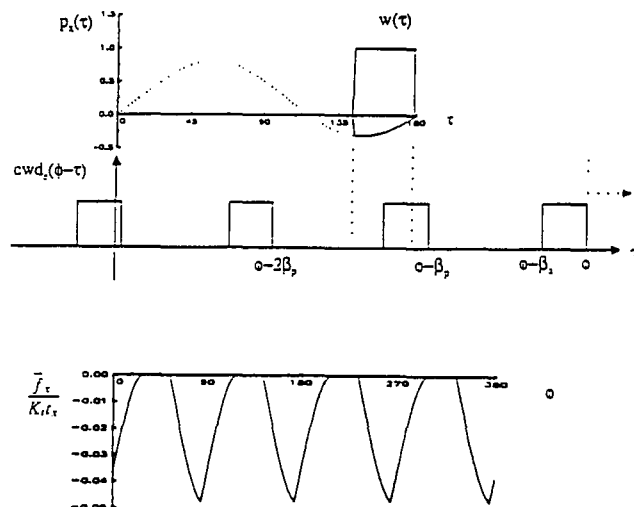
$$ts(\phi) = \sum_{k=-\infty}^{\infty} \delta(\phi - (k-1)\beta_p) \qquad (16)$$

where β_p is the angular spacing between neighboring flutes. The function shown in Fig. 3 is essentially a train of unit impulses separated by β_p and represents the rotation of the cutter and the successive engagement of each flute. The impulse for the kth flute is located at $\phi = (k-1)\beta_p$, which indicates the cutter rotation displacement when the leading edge of the kth flute passes through the point at $\theta = 0$.

2.4 Total Cutting Forces. The total cutting forces are the angular domain convolution of the tooth sequence function, the chip width density function, and the elementary cutting functions. Denoting convolution operation by "$*$", total cutting forces are expressed as:

$$\begin{pmatrix} \bar{f}_x(\phi) \\ \bar{f}_y(\phi) \end{pmatrix} = K_t t_x ts(\phi) * cwd(\phi) * \begin{pmatrix} p_x(\phi) \\ p_y(\phi) \end{pmatrix}$$

$$= K_t t_x \int_0^\phi \sum_{k=1}^\infty cwd[(\phi-\tau) - (k-1)\beta_p] \begin{pmatrix} p_x(\tau) \\ p_y(\tau) \end{pmatrix} d\tau \qquad (17)$$

This is a unified expression for the milling force system in the angular domain. A graphical representation of the convolution process and its resulting X component of the cutting force is given in Fig. 4.

3 Frequency Domain Model

From the property of convolution theorem, the frequency spectra of total cutting forces are the product of the frequency spectra of three process component functions. Therefore, the frequency characteristics of cutting forces can be studied by
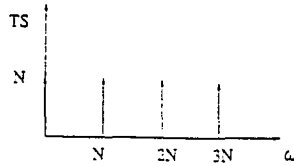
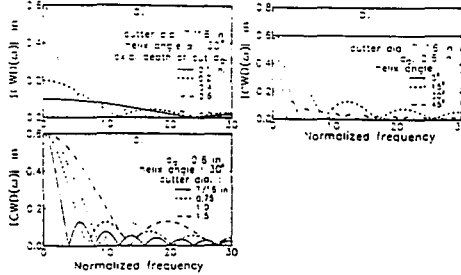Fig. 5 Spectrum plot of tooth sequence function, $TS(\omega)$

Fig. 6 Frequency spectra of chip width density function $CWD(\omega)$ for various cutter geometries

— :up-cut --- :entry angle 45° ····· :symmetry cut ·—· :down-cut
Cutter dia. 7/16 in., K_r: 0.5

Fig. 7 Frequency spectra of elementary cutting functions, $P_1(\omega)$ and $P_2(\omega)$, for various radial cutting geometries

examining the three model functions in the Fourier domain. In the following discussion, the transforms of these functions from the angular domain to the spectral domain is performed while the frequency variables are normalized with respect to the spindle rotation frequency. In other words a normalized frequency of ω in the following analysis is equivalent to ω times the spindle frequency.

3.1 Fourier Transform of Tooth Sequence Function.
The Fourier transform of the tooth sequence function can be shown from Eq. (16):

$$TS(\omega) = N \sum_{k=-\infty}^{\infty} \delta(\omega - Nk) \qquad (18)$$

Since $ts(\theta)$ is a periodic impulse sequence function in the angular domain, its Fourier transform is also a periodic discrete impulse function with a period of N as shown in Fig. 5. This implies that the cutting forces have non-zero frequency content only at the harmonics of the tooth passing frequency, Nk, in addition to their DC components.

3.2 Transform of Chip Width Density Function.
The Fourier transform of chip width density function can be derived as:

$$CWD(\omega) = \frac{2R}{\tan \alpha} \frac{\sin \dfrac{\omega}{N/\eta_a} \pi}{\omega} e^{-j\frac{\omega}{N/\eta_a}\pi} \qquad (19)$$

where

$$\eta_a = \frac{\beta_a}{\beta_p} = \frac{N d_a \tan \alpha}{2\pi R}$$

is the ratio of axial engagement angle to the tooth angular spacing angle. The magnitude of Fourier transform assumes the form of a sinc function, and is contained within an envelope which is inversely proportional to ω. Figure 6 (a, b, c) illustrates the effects of cutter geometry on the frequency spectrum of chip width density function. The effect of helical angle in reducing the cutting dynamics is clearly demonstrated in Fig. 6(b). It can be shown from Eq. (19) and is evident from these figures that the DC content of the spectrum is equal to the axial depth of cut. In addition, the spectrum has periodic zeros located at frequencies in multiples of $2\pi/\beta_a$ or N/η_a. Variations in cutter radius and helical angle will change η_a and hence zeroes of the spectrum. When η_a is an integer, frequencies at $\omega = kN$ are zeroes of the spectrum, and from Eq. (18) only

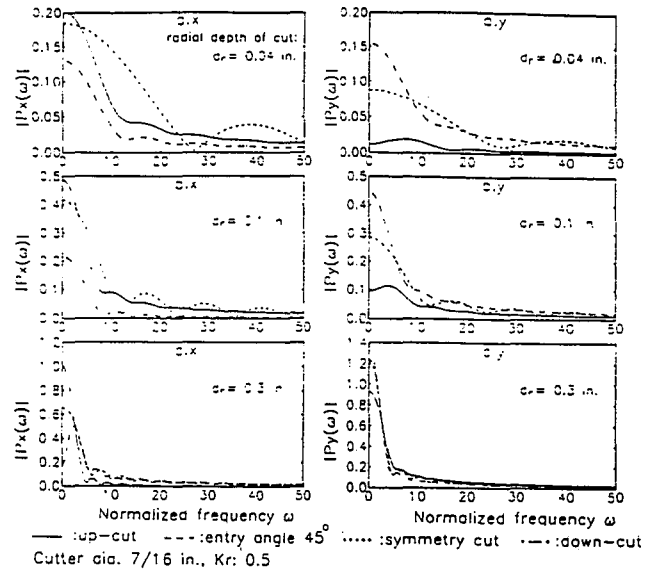signal contents at these frequencies are non-zero; therefore, the cutting forces will have only DC components.

3.3 Fourier Transforms of Elementary Cutting Functions.
The Fourier transforms of $p_x(\theta)$ and $p_y(\theta)$ in Eq. (8) are

$$\begin{pmatrix} P_x(\omega) \\ P_y(\omega) \end{pmatrix} = \begin{bmatrix} 1 & K_r \\ -K_r & 1 \end{bmatrix} \begin{pmatrix} P_1(\omega) \\ P_2(\omega) \end{pmatrix} \qquad (20)$$

$P_1(\omega)$ and $P_2(\omega)$ are the Fourier transforms of p_1 and p_2 in Eq. (13) and can be shown to be

$$P_1(\omega) = \frac{1}{2(4-\omega^2)} [(e^{-j\omega\theta_{1r}}(j\omega \sin 2\theta_{1r} + 2 \cos 2\theta_{1r})$$
$$- e^{-j\omega\theta_{2r}}(j\omega \sin 2\theta_{2r} + 2 \cos 2\theta_{2r})] \qquad (21)$$

$$P_2(\omega) = \frac{e^{-j\omega\theta_{1r}} - e^{-j\omega\theta_{2r}}}{j2\omega}$$
$$- \frac{1}{2(4-\omega^2)} [e^{-j\omega\theta_{1r}}(j\omega \cos 2\theta_{1r} - 2 \sin 2\theta_{1r})$$
$$- e^{-j\omega\theta_{2r}}(j\omega \cos 2\theta_{2r} - 2 \sin 2\theta_{2r})] \qquad (22)$$

The frequency spectrum of the elementary cutting functions are shown in Fig. 7 for three values of d_r under various radial cutting configurations. For each d_r, spectra for four different cutting configurations are obtained. It is seen in the figures that the position of the workpiece relative to the cutter has significant effects on the dynamics of the cutting force system, especially when the radial depth of cut is small. The position and width of the window function $w(\theta)$, defined by the entry and exit angles, subtly affects the spectra of these two elementary cutting functions. It can be shown that if the cutting window is located such that the elemental force has a symmetric shape, its spectrum will have clearly defined peaks and valleys and a high DC content similar to the frequency response of a low pass filter. On the other hand, if the elemental force has an anti-symmetric shape, its spectrum will have a low DC component and higher dynamic content similar to a high pass filter response. These statements are evidenced by the spectra shown in Fig. 7.

3.4 Fourier Transforms of the Total Cutting Forces.
From the convolution representation of the total cutting forces in Eq. (17), the Fourier transforms of the total cutting forces are
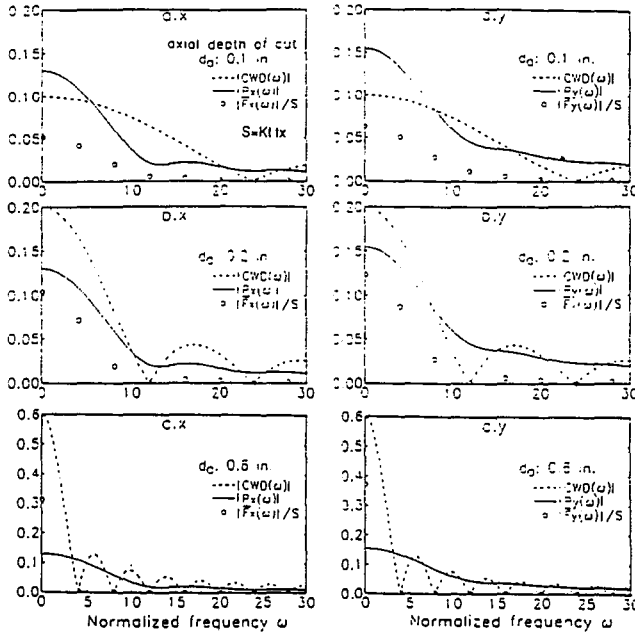
Fig. 8 Frequency spectra of total cutting forces $\bar{F}_f(\omega) = K_t t_x TS(\omega)$ $CWD(\omega)P_i(\omega)$. Circles represent the areas of spectral impulses. Assumed cutting conditions are: cutter dia. = 7/16 in., helical angle = 30 deg., $N = 4$, $d_r = 0.04$ in., $K_r = 0.5$, down cut

the product of the transforms of the elementary cutting function, the chip width density function, the tooth sequence function, and the constant $K_t t_x$. That is,

$$\begin{pmatrix} \bar{F}_x(\omega) \\ \bar{F}_y(\omega) \end{pmatrix} = K_t t_x TS(\omega) CWD(\omega) \begin{pmatrix} P_x(\omega) \\ P_y(\omega) \end{pmatrix}$$

$$= K_t t_x N \sum_{k=-\infty}^{\infty} \delta(\omega - Nk) CWD(\omega) \begin{bmatrix} 1 & K_r \\ -K_r & 1 \end{bmatrix} \begin{pmatrix} P_1(\omega) \\ P_2(\omega) \end{pmatrix}$$

(23)

The total cutting force in the angular domain can be expressed in a more useful form using Fourier integral formula:

$$\begin{pmatrix} \bar{f}_x(\phi) \\ \bar{f}_y(\phi) \end{pmatrix} = \frac{1}{2\pi} \int_{-\infty}^{\infty} \begin{pmatrix} \bar{F}_x(\omega) \\ \bar{F}_y(\omega) \end{pmatrix} e^{j\omega\phi} d\omega$$

$$= \frac{NK_t t_x}{2\pi} \int_{-\infty}^{\infty} \sum_{k=-\infty}^{\infty} \delta(\omega - Nk) CWED(\omega)$$

$$\times \begin{bmatrix} 1 & K_r \\ -K_r & 1 \end{bmatrix} \begin{pmatrix} P_1(\omega) \\ P_2(\omega) \end{pmatrix} e^{j\omega\phi} d\omega$$

$$= \sum_{k=-\infty}^{\infty} \begin{pmatrix} A_x[Nk] \\ A_y[Nk] \end{pmatrix} e^{jNk\phi}$$

(24)

where

$$\begin{pmatrix} A_x[Nk] \\ A_y[Nk] \end{pmatrix} = \frac{NK_t t_x}{2\pi} CWD(Nk) \begin{bmatrix} 1 & K_r \\ -K_r & 1 \end{bmatrix} \begin{pmatrix} P_1(Nk) \\ P_2(Nk) \end{pmatrix}$$

(25)

are the coefficients of the Fourier series expansion of $\bar{f}_x$ and $\bar{f}_y$, and are expressed explicitly as the algebraic functions of cutting parameters. Once the Fourier coefficients of the cutting forces are available, the angular domain force profile can be computed very efficiently using standard inverse FFT routine.

Figure 8 illustrates the generation of frequency spectra for the total cutting forces from the three process components functions. The total cutting forces have non-zero components at $\omega = Nk$ as a result of $TS(\omega)$ in Eq. (18); spectra magnitude
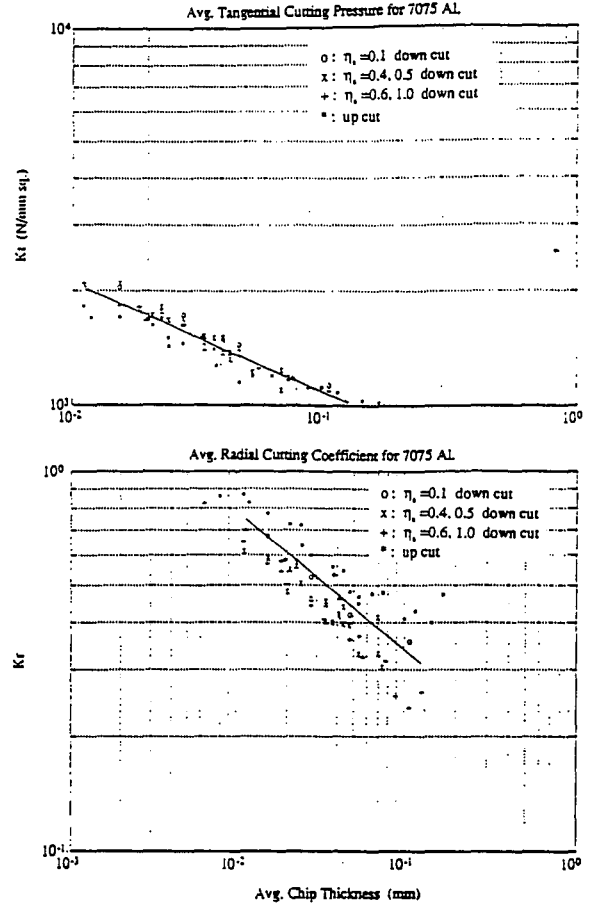

Fig. 9 (a) average tangential and (b) average radial cutting constants vs. average chip thickness, t_c

at these frequencies is modulated by values of P_1, P_2, and CWD at respective frequencies. Scaled total cutting force frequency spectra are calculated based on Eq. (23) and shown as circles in the figure for three cutting cases each with different axial depth of cut. The last case in Figure 8(c) was calculated with a cutter engagement angle β_a being equivalent to tooth pitch angle β_p, i.e., $\eta_a = 1$. In this particular case a constant cutting force without any dynamic frequency component results as expected. The average cutting forces at $\omega = 0$ are shown to be proportional to the axial depth of cut.

4 Experimental Verification and Discussions

A series of end milling experiments were conducted to evaluate the validity of the analytical frequency domain model. Cutting was performed with 7075-T6 aluminum on a vertical milling machine. The cutting force data from a Kistler dynamometer were digitized at every degree of cutter rotation. Ten cycles of data are collected and transformed into the frequency domain using standard FFT software. For each cutting configuration, average cutting pressure constants K_t and K_r of the process were obtained from the average X and Y forces of the experimental cutting force data. It can be shown from Eq. (25) that

$$\begin{pmatrix} K_t \\ K_t K_r \end{pmatrix} = \begin{bmatrix} P_1(0) & P_2(0) \\ P_2(0) & -P_1(0) \end{bmatrix}^{-1} \begin{pmatrix} A_x[0] \\ A_y[0] \end{pmatrix} \frac{2\pi}{Nt_x d_a}$$

(26)

in which $A_x[0]$ and $A_y[0]$ are the measured average forces and $P_1(0)$ and $P_2(0)$ are from Eqs. (21, 22) with $\omega = 0$.

Cutting tests were taken with various radial and axial cutting configurations. Average cutting pressure constants from these cutting tests are related to the average chip thickness and shown in Figs. 9(a) and 9(b). Clearly, a definite relationship can be

Table 1 Cutting conditions and comparisons of cutting force dynamic components from experimental and theoretical results. Material: 7075–T6 aluminum: cutter geometry: $N = 4$, $D = 5/8$ in., (15.875 mm), flute length: 1.75 in. (44.45 mm), helical angle: 30 deg.; cutting speed: 135 rpm, no coolant, sampling rate: 360 per rev

No.	Cutting Conditions							Meas. Avg.		M²/P²	Cutting Const.		X force Dynamic Fourier Coeff.				Y force Dynamic Fourier Coeff.			
	Type of cut[1]	η_t (d/D)	η_a (β_t/β_a)	t_t (10⁻³)	f_t (10⁻³)	$A_x[0]$ (N)	$A_y[0]$ (N)				K_t (N/mm sq.)	K_r	$A_x[4]$ Mag. (N)	$A_x[4]$ Phase (Deg.)	$A_x[8]$ Mag. (N)	$A_x[8]$ Phase (Deg.)	$A_y[4]$ Mag. (N)	$A_y[4]$ Phase (Deg.)	$A_y[8]$ Mag. (N)	$A_y[8]$ Phase (Deg.)
5	1	0.2	0.4	64.3	27.7	-129.47	221.36	1	1,688.7	0.46	60.25	226.33	0.64	323.76	97.49	69.03	6.53	222.1
								2	1,570.02	0.54	64.09	230.45	2.84	312.77	118.35	78.78	14.76	194.79
6	1	0.2	0.6	64.3	27.7	-189.42	312.56	1	1,615.82	0.44	60.6	195.76	2.3	73.92	95.94	39.85	12.11	315.07
								2	1,570.02	0.54	62.46	195.22	2.81	64.73	111.62	43.02	13.97	302.96
11	1	0.3	1	172.3	89.2	-841.13	1,328.89	1	1,113.97	0.26	11.07	271.77	1.09	128.38	7.36	169.94	2.33	184.56
								2	1,127.9	0.35	0		0		0		0	
15	1	0.6	0.5	35.7	24.2	6.88	504.43	1	1,675.97	0.5	69.84	239.52	2.63	343.56	44.71	204.4	2.55	197.64
								2	1,631.88	0.57	78.24	246.29	0.01	187.38	72.46	198.01	0.01	172.29
19	0	0.05	0.6	64.3	14.3	108.6	-36.51	1	1,761.22	0.72	44.6	201.91	12.53	207.28	14.7	65.24	5.04	52.66
								2	1,895	0.69	50.15	181.91	11.76	180.76	16.7	10.77	3.76	20.09
22	0	0.1	0.37	172.3	53.6	231.88	-2.65	1	1,198.82	0.47	148.56	301.39	29.07	231.18	24.7	221.07	11.33	179.19
								2	1,303.01	0.43	151.26	193.52	32.38	16.47	14.57	107.34	7.26	312.69
16	1	1	0.43	64.3	40.9	377.84	810.97	1	1,376.29	0.47	37.05	191.98	4.56	8.08	48.48	40.11	5.94	355.54
								2	1,406.27	0.47	0		0		0		0	
18	2	0.6	0.43	64.3	43.5	244.89	557.52	1	1,322.85	0.44	116.26	355.29	13.09	93.99	106.93	273.85	18.43	46.7
								2	1,381.92	0.46	118.11	348.12	8	68.66	124.67	261.5	13.83	17.45

Note 1: 0,1 and 2 for up, down and symmetric cut.   Note 2: M.: measured.   P.: predicted.

expressed using exponential equations like (3) and (5) for K_t and K_r. Two straight lines shown in Fig. 9 are fitted on the log-log plot for K_t and K_r of this cutter/work combination and can be expressed as

$$K_t = 569.14(\bar{t}_c)^{-0.283} \quad \text{N/mm}^2 \tag{27}$$

$$K_r = 0.1468(\bar{t}_c)^{-0.364} \tag{28}$$

where $\bar{t}_c$ can be expressed as

$$\bar{t}_c = \frac{2\eta_r}{\theta_{rr}} \tag{29}$$

The average chip thickness in the presence of cutter axial offset needs to be modified according to Kline et al. (1983) and Wang (1992). Since the offset is small in these cutting tests, it is found that its effect on the average chip thickness is insignificant. The magnitude of these cutting constants are within the range reported by Kline et al. (1983) and Altintas and Spence (1991).

Table 1 summarizes the cutting conditions and experimental and analytical results for eight cases of the cutting tests. The predicted K_t and K_r from Eqs. (27, 28) are compared with experimental results. The model-predicted dynamic Fourier series coefficients were calculated by substituting the experimental K_t and K_r into Eq. (25). Since the spindle frequency is 2.25 Hz, the normalized frequencies of $\omega = 4$, 8 and 12 in $A_x[\omega]$ and $A_y[\omega]$ correspond to 9, 18 and 27 Hz in the experimental data. The Fourier series coefficients of the measurement data and those from the analytical model are compared at the first harmonic, the second harmonic, and the third harmonic of the tooth passing frequency (9 Hz) and are shown in Fig. 10. The experimental data are shown in solid line with the average forces marked with x. The predicted dynamic Fourier coefficients are given by o. It is shown that the results from experiments agree well in magnitude and phase with that from the analytical model.

For $\eta_a = 1$ in case (3), cutting forces do not have dynamics components as predicted in Fig. 8(c). Consequently, the dynamic components for $\eta_a = 0.4$ and (1-0.4) in cases (1, 2) should have the same magnitude given that other cutting conditions are the same, and their average force are proportional to the axial depth of cut as the experiment results show. Dynamic components also vanish in the full cut configuration with $\eta_r = 1$ for a four-flute cutter as in case (7); this can be proven by showing the $P_1(\omega)$ and $P_2(\omega)$ and $P_x(\omega)$ and $P_y(\omega)$ in Eqs. (20–22) have zeroes at $\omega = \pm 4$, ± 6, ± 8 . . . with $\eta_r = 1$. Since the constant cutting constants in the model is an approximation, the experimental data still show a small magnitude of cutting forces in their dynamic components; for the case with $\eta_a = 1$, the reason for zero dynamic components is in the chip width density function of the cutter, which is geometrical in nature and is not an approximation. Therefore the prediction of zero dynamic component from the model with $\eta_a = 1$ tends to be more accurate.

Among all cutting configurations, the worst percentage error in the dynamic components occur when very small average cutting forces are encountered. Small average X force exists in down cut at around $\eta_r = 0.1$ while small average Y force occurs in up cut at around $\eta_r = 0.6$; the exact value of η_r at which zero average cutting forces exist depends on the value of K_r and indirectly on the feed per tooth (Wang, 1992). Cases (4) and (6) have such two cutting conditions and the large percentage error in the prediction of dynamic components are observed in Fig. 10(a) for case (4) and Fig. 10(b) for case (6). However, the magnitude of these differences is very small and can be considered insignificant compared to the cutting force in the other direction. Close comparisons are obtained from symmetric cut configurations for all range of η_r. Figure 10(b) for case (8) shows the results from one of the symmetric cutting tests.

Notice that spectrum peaks occur at spindle frequency and at frequencies which are one spindle frequency above and below the harmonics frequencies as a result of cutter runout. Kline et al. (1983) have reported the effect of cutter runout on the shifting of cutting force from tooth passing frequency to spindle frequency. The detailed analysis of cutter runout effect has been summarized in Wang (1992).

The accuracy of the model in predicting dynamic components is shown to be well supported by the experimental data. The validity of cutting force models in predicting average cutting forces using expressions such as Eqs. (27) and (28) for other cutting configurations has been reported by other researchers (Kline et al., 1982; Fussel, Srinivasan, 1989; Yusesan et al., 1990). However, the effect of using such constant K_t and K_r on the dynamic components of the cutting forces has not been analyzed.
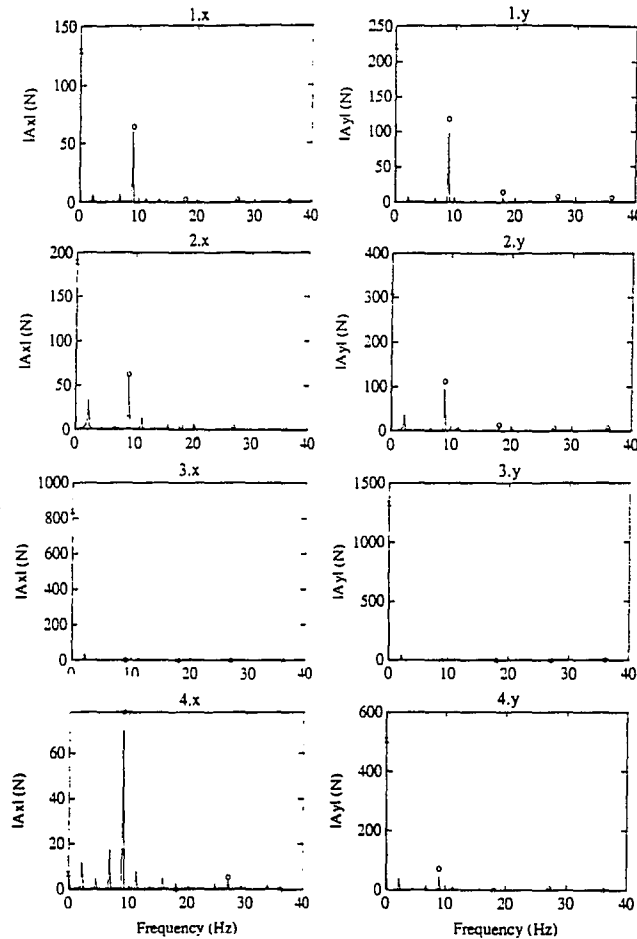
Fig. 10(a) Frequency spectra of measured and predicted forces (given by o) for cases (1–4) in Table 1. x indicates the average forces.
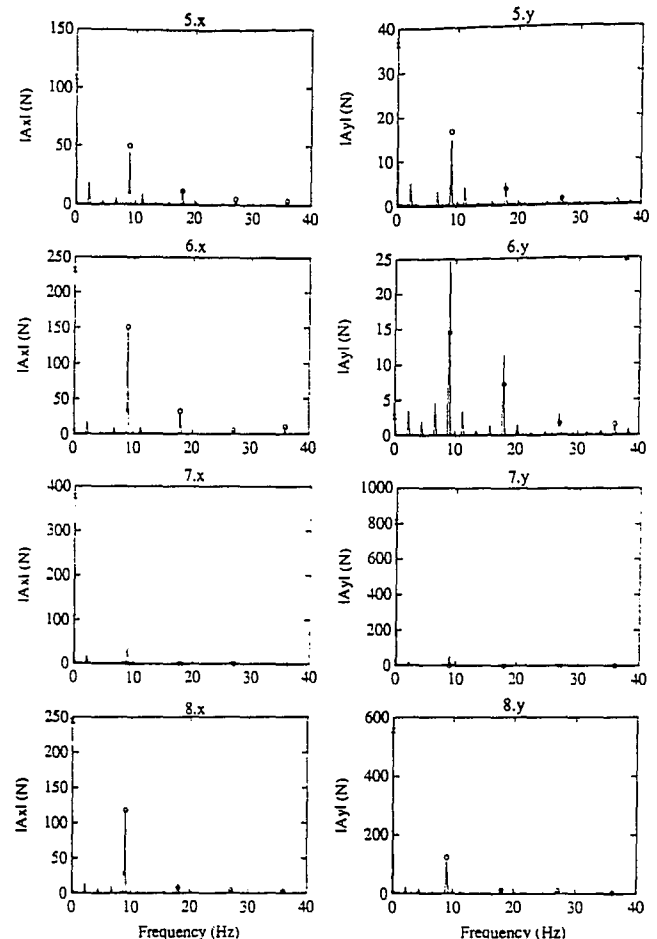

Fig. 10(b) Frequency spectra of measured and predicted forces (given by o) for cases (5–8). x indicates the average forces.

If the cutting pressure constants are obtained strictly from the average forces, it should then be expected that errors exist in using these constant process parameters to predict the Fourier coefficients of the dynamic components of cutting forces. It is therefore necessary to investigate to what extent such an approximation will affect the accuracy of the model. Following from Eqs. (2), (3), (27) and (28), the true variable cutting pressure coefficients for the local cutting forces take the exponential forms of:

$$k_t = 569.14(t_c)^{-0.283} \text{ N/mm}^2 \tag{30}$$

$$k_r = 0.1468(t_c)^{-0.364} \tag{31}$$

Note the lower cases k_t and k_r are used to represent the non-constant values of cutting pressure coefficients. The true or ideal local cutting forces are expressed as

$$\begin{pmatrix} f_{x1}(\theta) \\ f_{y1}(\theta) \end{pmatrix} = k_t(\theta) t_x \begin{bmatrix} 1 & k_r(\theta) \\ -k_r(\theta) & 1 \end{bmatrix} \begin{pmatrix} p_1(\theta) \\ p_2(\theta) \end{pmatrix} \tag{32}$$

If K_t and K_r are truly constant, the total cutting forces calculated from the integration of Eq. (32) should be identical to those obtained based on Eqs. (17) and (26). In this study, the difference between cutting forces evaluated on these two different bases have been examined in appraising the constant K_t and K_r assumption. For each case in Table 1, the average cutting pressure constants are calculated from the following equation:

$$\begin{pmatrix} K_t \\ K_t K_r \end{pmatrix} = \begin{bmatrix} P_1(0) & P_2(0) \\ P_2(0) & -P_1(0) \end{bmatrix}^{-1} \begin{pmatrix} F_{x1}(0) \\ F_{y1}(0) \end{pmatrix} \frac{1}{t_x} \tag{33}$$

where $F_{x1}(0)$ and $F_{y1}(0)$ are the DC components of Fourier

transforms of $f_{x1}(\theta)$ and $f_{y1}(\theta)$ and can be obtained from numerical integration. Equation (30) is similar to Eq. (26) except that only local cutting forces are considered here. The same K_t and K_r should be obtained if total cutting forces for a certain cutter geometry and axial depth of cut are simulated and Eq. (26) is used to calculate K_t and K_r. The approximated local cutting forces are then expressed as

$$\begin{pmatrix} f_x(\theta) \\ f_y(\theta) \end{pmatrix} = K_t t_x \begin{bmatrix} 1 & K_r \\ -K_r & 1 \end{bmatrix} \begin{pmatrix} p_1(\theta) \\ p_2(\theta) \end{pmatrix} \tag{34}$$

Two of the simulation results are shown for cases (1) and (6) in Fig. 11(a, b). Solid lines are for the ideal cutting forces in part (i) and their frequency spectra in part (ii) of these figures. The interpretation of these frequency spectra is similar to that for the spectrum plots of P_x and P_y in Fig. 8. The spectra of total forces will be located at Nk and modulated by the spectrum of chip width density function. The spectra of these two cutting cases in Fig. 11 match very well with their respective spectra in Fig. 10. This indicates that the error observed in Fig. 10 can be largely attributed to the use of constant K_t and K_r in the analytical model. Additional simulation results with various radial cutting configurations show that the differences in the magnitude and phases of force spectra are small, and these differences also reflect the discrepancies shown in Fig. 10. These results suggest that the use of constant cutting pressure coefficients is reasonably adequate in capture the overall dynamics of the local cutting forces and the total cutting forces.

5 Summary

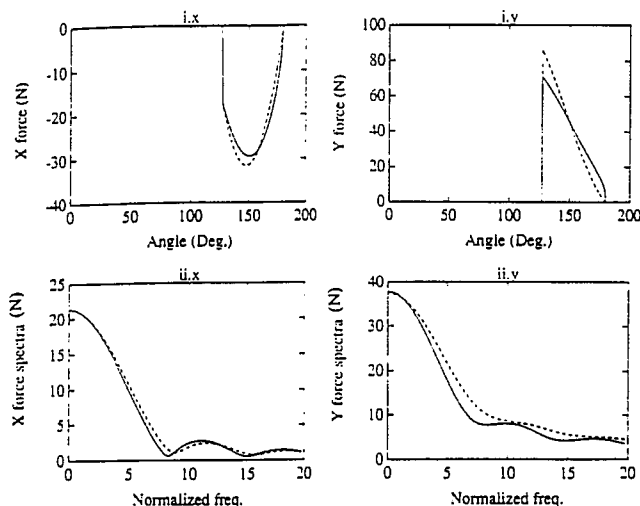In this work, the total cutting forces in milling processes

Fig. 11(a) Local cutting forces with constant (solid line) and variable cutting coefficients for cutting case (1)
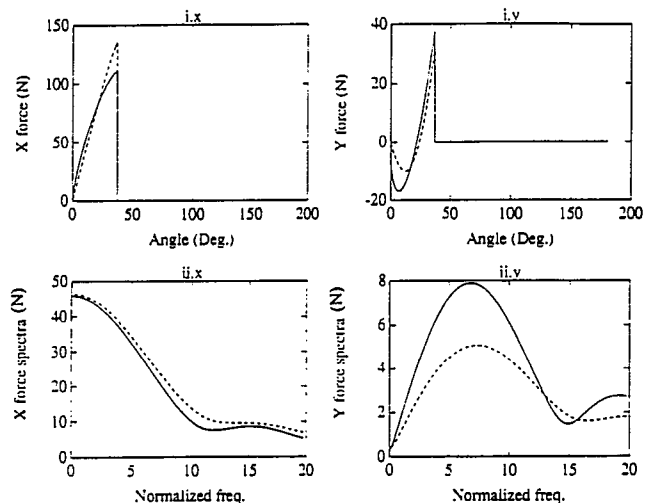

Fig. 11(b) Local cutting forces with constant (solid line) and variable cutting coefficients for cutting case (6)

have been derived as the angular convolution of three component functions, namely the elementary cutting function, the chip width density function, and the tooth sequence function. A closed form expression in the frequency domain for the cutting forces was thus derived as explicit functions of cutting conditions and tool/workpiece geometry. The analysis of the total cutting forces was performed by deriving and discussing the frequency transforms of the three component functions. Each process component is characterized with a unique frequency spectrum which can be related to specific cutting parameters. The tooth sequence function specifies the frequencies $\omega = 0$, $\pm Nk$, at which force components exist. The chip width density function has a DC component value of d_a and its spectrum is a sinc function with zeroes located at multiples of N/η_a. Fourier series coefficients of the cutting forces were shown to be algebraic functions of various tool parameters and cutting conditions.

A series of end milling experiments along with numerical simulation were performed to validate the analytical model. The Fourier series coefficients of the measured forces agrees well with the predictions from the model. In addition, the close agreement between cutting forces calculated based on K_t and K_r from the average forces and based on variable k_t and k_r suggests that constant K_t and K_r assumption presented limited infidelity in the modeling of dynamic cutting force components.

References

Altintas, Y., and Spence, A., 1991, "End Milling Force Algorithms for CAD Systems," *CIRP Annals*, Vol. 40.

Armarego, E. J. A., and Deshpande, N. P., 1989, "Computerized Predictive Cutting Model for Cutting Forces in End-Milling Including Eccentricity Effects," *CIRP Annals*, Vol. 38.

Armarego, E. J. A., and Deshpande, N. P., 1991, "Computerized End-Milling Force Prediction with Cutting Models Allowing for Eccentricity and Cutter Deflections," *CIRP Annals*, Vol. 40.

Ber, A., Rotberg, J., and Zombach, S., 1988, "A Method for Cutting Force Evaluation of End Mills," *CIRP Annals*, Vol. 37.

Fu, H. J., DeVor, R. E., and Kapoor, S. G., 1984, "A Mechanistic Model for the Prediction of the Force System in Face Milling Operation," ASME JOURNAL OF ENGINEERING FOR INDUSTRY, Vol. 106, pp. 81–88.

Fussel, B. K., and Srinivasan, K., 1989, "An Investigation of the End Milling Process Under Varying Machining Conditions," ASME JOURNAL OF ENGINEERING FOR INDUSTRY, Vol. 111, pp. 27–36, Feb.

Gygax, P. E., 1989, "Experimental Full Cut Milling Dynamics," *CIRP Annals*, Vol. 29, pp. 61–66.

Gygax, P. E., 1979, "Dynamics of Single-Tooth Milling," *CIRP Annals*, Vol. 28, pp. 65–70.

Kato, S., Yamada, T., Hashimoto, M., and Yamaguchi, K., 1981, "Relationships Between Cutting Force Vibrations and Cutting Factors in Plain Milling Operations. Part 1: Plain Milling With a Single-Toothed Helical Cutter," ASME JOURNAL OF ENGINEERING FOR INDUSTRY, Vol. 103, pp. 165–173, May.

Kato, S., Yamada, T., Hashimoto, M., and Yamaguchi, K., 1981, "Relationships Between Cutting Force Variations and Cutting Factors in Plain Milling Operations. Part 2: Plain Milling With a Multi-Toothed Helical Cutter," ASME JOURNAL OF ENGINEERING FOR INDUSTRY, Vol. 103, pp. 174–182, May.

Kline, W. A., DeVor, R. E., and Lindberg, J. R., 1982, "The Prediction of Cutting Forces in End Milling with Application to Cornering Cut," *International Journal of Machine Tool Design and Research*, Vol. 22, pp. 7–22.

Kline, W. A., and DeVor, R. E., 1983, "The Effect of Runout on Cutting Geometry and Forces in End Milling," *International Journal of Machine Tool Design and Research*, Vol. 23, No. 2/3, pp. 123–140.

Koenigsberger, F., and Sabberwal, A. J. P., 1961, "An Investigation into the Cutting Force Pulsations During Milling Operations," *International Journal of Machine Tool Design and Research*, Vol. 1, pp. 15–33.

Martellotti, M. E., 1945, "An Analysis of the Milling Process, Part 2: Down Milling," *Transactions of the ASME*, Vol. 67, pp. 233–251.

Martellotti, M. E., 1941, "An Analysis of the Milling Process," *Transactions of the ASME*, Vol. 63, pp. 677–700.

Sabberwal, A. J. P., 1962, "Cutting Forces in Down Milling," *International Journal of Machine Tool Design and Research*, Vol. 2, pp. 27–41.

Sabberwal, A. J. P., 1961/62, presented by F. Koenigsberger, "Chip Section and Cutting Force During the Milling Operation," *CIRP Annals*, Vol. 10, pp. 197–203.

Subramani, G., Suvada, R., Kapoor, S. G., DeVoor, R. E., and Meingast, W., 1987, "A Model for the Prediction of Force System for Cylinder Boring Process," *Proceedings of the 15th NAMRC*, Vol. 2, pp. 439–446.

Sutherland, J. W., and DeVor, R. E., 1986, "An Improved Method for Cutting Force and Surface Error Prediction in Flexible End Milling Systems," ASME JOURNAL OF ENGINEERING FOR INDUSTRY, Vol. 108, pp. 269–279, Nov.

Tlusty, J., and MacNeil, P., 1975, "Dynamics of Cutting Forces in End Milling," *CIRP Annals*, Vol. 24, pp. 21–25.

Wang, J.-J., 1992, "Convolution Modelling of Milling Force System and Its Application to Cutter Runout Identification," Ph.D. Thesis, Georgia Institute of Technology, Apr.

Wang, J.-J., Liang, S. Y., and Book, W. J., 1991, "Analysis of Milling Forces via Angular Convolution," *Sensors, Controls, and Quality Issues in Manufacturing*, PED-Vol. 55, pp. 135–150, ASME Winter Annual Meeting, Atlanta, GA, Dec.

Yucesan, G., Bayoumi, A. E., and Kendall, L. A., 1990, "An Analytic Cutting Force Model for Milling," *Transactions of NAMRI/SME*, pp. 137–145.

Zhou, R., and Wang, K. K., 1983, "Modelling of Cutting Force Pulsation in Face-Milling," *CIRP Annals*, Vol. 32.